OC6 Phase III Definition Document

Amy Robertson,[1] Roger Bergua,[1] Alessandro Fontanella,[2] and Jason Jonkman[1]

1 National Renewable Energy Laboratory
2 Politecnico di Milano

NREL is a national laboratory of the U.S. Department of Energy
Office of Energy Efficiency & Renewable Energy
Operated by the Alliance for Sustainable Energy, LLC

This report is available at no cost from the National Renewable Energy Laboratory (NREL) at www.nrel.gov/publications.

Contract No. DE-AC36-08GO28308

Technical Report
NREL/TP-5000-83102
February 2023

OC6 Phase III Definition Document

Amy Robertson,[1] Roger Bergua,[1] Alessandro Fontanella,[2] and Jason Jonkman[1]

1 National Renewable Energy Laboratory
2 Politecnico di Milano

Suggested Citation
Robertson, Amy, Roger Bergua, Alessandro Fontanella, Jason Jonkman. 2023. *OC6 Phase III Definition Document*. Golden, CO: National Renewable Energy Laboratory. NREL/TP-5000-83102. https://www.nrel.gov/docs/fy23osti/83102.pdf.

NREL is a national laboratory of the U.S. Department of Energy
Office of Energy Efficiency & Renewable Energy
Operated by the Alliance for Sustainable Energy, LLC

This report is available at no cost from the National Renewable Energy Laboratory (NREL) at www.nrel.gov/publications.

Contract No. DE-AC36-08GO28308

Technical Report
NREL/TP-5000-83102
February 2023

National Renewable Energy Laboratory
15013 Denver West Parkway
Golden, CO 80401
303-275-3000 • www.nrel.gov

NOTICE

This work was authored in part by the National Renewable Energy Laboratory, operated by Alliance for Sustainable Energy, LLC, for the U.S. Department of Energy (DOE) under Contract No. DE-AC36-08GO28308. Funding provided by the U.S. Department of Energy Office of Energy Efficiency and Renewable Energy Wind Energy Technologies Office. The views expressed herein do not necessarily represent the views of the DOE or the U.S. Government.

Cover Photos by Dennis Schroeder: (clockwise, left to right) NREL 51934, NREL 45897, NREL 42160, NREL 45891, NREL 48097, NREL 46526.

List of Acronyms

CP	coefficient of power
CS	coordinate system
CT	coefficient of thrust
deg	degree
DTU	Technical University of Denmark
IRPWind	Integrated research programme on wind energy
kg	kilogram
kHz	kilohertz
LC	load case
m	meter
mm	millimeter
MW	megawatt
N	newton
NREL	National Renewable Energy Laboratory
OC6	Offshore Code Comparison Collaboration, Continued, with Correlation and unCertainty
PIV	particle image velocimetry
Polimi	Politecnico di Milano
rpm	revolutions per minute
s	second
TNO	Netherlands Organisation for Applied Scientific Research
UNAFLOW	UNsteady Aerodynamics for FLOating Wind

Table of Contents

List of Figures

List of Tables

1 Objective

The objective of Phase III of the Offshore Code Comparison Collaboration, Continued, with Correlation and unCertainty (OC6) project was to evaluate the accuracy of aerodynamic load predictions by offshore wind modeling tools for a floating offshore wind turbine as it experiences large surge-translational and pitch-rotational motion, as would occur during normal operation. A variety of models were examined in the project, with the goal of performing a three-way validation between engineering-level tools, higher-fidelity tools, and measurement data from two wind tunnel experimental campaigns.

This document provides the necessary information to model and simulate the system studied in the OC6 Phase III project. This information is not only useful for project participants, but also future modelers who want to replicate this work for verification and validation purposes.

2 Experimental Campaign

2.1 Overview

The first data set that was used in OC6 Phase III was developed in the UNsteady Aerodynamics for FLOating Wind (UNAFLOW) project, which was a collaborative effort under the European Union's Integrated Research Programme on Wind Energy (IRPWind) and included Politecnico di Milano (Polimi), the Energy Research Centre of the Netherlands (now part of the Netherlands Organisation for Applied Scientific Research, or TNO), University of Stuttgart, and the Technical University of Denmark (DTU) (Bernini et al. 2017). The testing was essentially a repeat of similar testing performed as part of the LIFES50+ project[1], but with a stiffer tower and a 5-degree (deg) tower tilt to make the rotor vertical (offsetting the rotor tilt). The flexible tower in LIFES50+ created issues in the measurements, making validation difficult.

Additional tests that were used in this study were conducted by Polimi at their facility during the summer of 2021. The tests during this follow-on campaign reproduced some tests from the UNAFLOW campaign (e.g., steady wind conditions and some forced oscillations in the surge direction) and included forced oscillation in the platform pitch direction.

2.2 Test Facility

All testing was conducted in the Polimi wind tunnel boundary layer test section (see Figure 1), which is 13.84 meters (m) wide by 3.84 m high by 35 m long. The air density in the facility can be considered equal to 1.177 kilograms per cubed meter (kg/m^3) during both test campaigns. The tests were performed using an empty inlet configuration (i.e., without roughness elements or turbulence generators) for a constant inflow velocity and a resulting turbulence intensity around 2% (see Figure 2). Two rows of seven 2 × 2-m independent fans were used, producing a total fan power of 1.4 megawatts (MW).

Figure 1. Polimi wind tunnel during the UNAFLOW project with scaled DTU 10-MW reference wind turbine. *Image from Alessandro Fontanella, Politecnico di Milano*

[1] *LIFES50+ is a research project funded by the European Union Horizon2020 programme. It focuses on floating substructures for 10-megawatt wind turbines at water depths greater than 50 meters (https://lifes50plus.eu/).*

2.3 Scaled Turbine Design

The test turbine is a 1:75 scaled version of the DTU 10-MW reference wind turbine (Bak et al. 2013), which was designed by Polimi within the LIFES50+ project. It is a variable-speed wind turbine with individual blade-pitch control. The scaling approach for the turbine sought to preserve the coefficient of thrust (CT) and coefficient of power (CP) of the full-scale design while scaling the overall physical dimensions by a 1:75 factor. The structural design itself was driven by mass scaling.

To achieve the scaling objectives, the wind velocity was scaled by a factor of 3, and a low-Reynolds-number airfoil (SD7032) was used because the Reynold's number in the wind tunnel was 225 times smaller than full scale. The blade chord and twist distributions were altered to achieve the correct thrust forces and to match the torque adequately up to rated conditions (Bayati et al. 2017).

During the UNAFLOW project, the turbine was mounted on a test rig with two hydraulic actuators at the tower base to enable forced motion of the turbine in the surge direction (see Figure 1). In the follow-on campaign, the turbine was mounted atop a 6-degrees-of-freedom robot. The overall properties of the scaled turbine are given in Table 1. All model information in this document is given at model scale.

2.4 Wind Quality

The goal of the experimental campaign was to get as uniform a flow as possible. However, perfectly uniform wind flow is not possible due to the influence of the tunnel walls and the turbulence generated from the fans. Figure 2 shows the measured vertical wind speed profile (*U*), normalized by the wind speed at hub height (*Uref*), and the turbulence intensity, which is close to 2% in the region covered by the rotor.

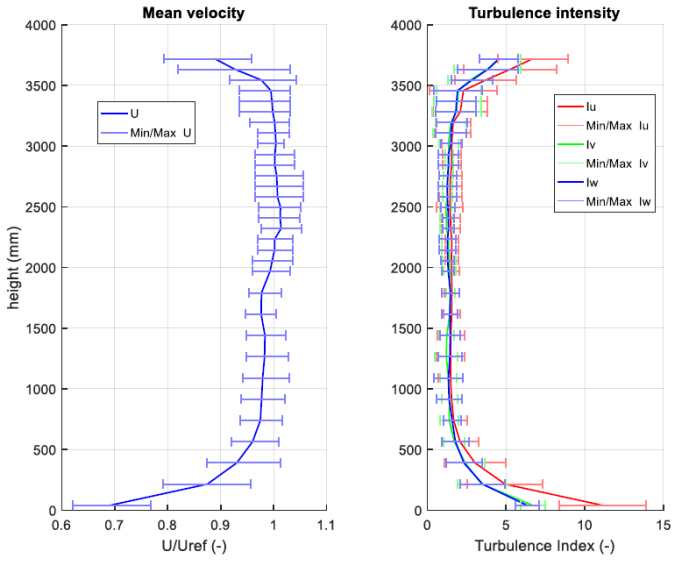

Figure 2. Polimi wind tunnel flow characteristics (Bernini et al. 2017). During testing, the turbine lies around the 1–3 m range across this height (hub height near 2 m).

I refers to the turbulence intensity in the longitudinal (u), transverse (v), and vertical (w) directions

2.5 Measurements

The measurements taken during the UNAFLOW test campaign are as follows (output channels summarized in Appendix A.1):

- 6-degrees-of-freedom load cell at top of tower
- 6-degrees-of-freedom load cell at bottom of tower, between tower and moving platform
- Particle image velocimetry (PIV) for some cases: measures two velocity components (axial and vertical) and vorticity of the wake in the vertical plane behind the turbine (see Bayati et al. [2018] for more details)
- Surge position by laser transducer
- Hot-wire probe.

The measurements taken during the follow-on campaign only include the tower top loads and the platform surge and pitch positions.

All measurements were sampled at 2 kilohertz (kHz) and windowed to avoid leakage. All data were stored at model scale, and similarly, all information in this document is presented at model scale, unless otherwise noted. As such, simulations were also performed at model scale.

To obtain aerodynamic thrust and torque, the inertial components were removed from the force measurements.

2.6 Testing Issues

In this test setup, there was some difficulty in getting the aerodynamic thrust from the measurements. The measured load signal was heavily affected by nacelle inertia from acceleration. To subtract this component, measurements were also performed without wind. However, some flexibility in the tower complicated this subtraction process. The UNAFLOW project used a stiffer tower than what was used in the LIFES50+ project to help address this issue. In addition, filtering was applied to eliminate high-frequency components due to tower dynamics, imperfect surge excitation, rotor dynamic effects, aerodynamic turbulence, and measurement noise.

3 Model Information

This section provides the information needed to build the two simulation models of the scaled turbines tested at Polimi. Previous modeling work based on the UNAFLOW test can be found in references from Cormier et al. (2018) and Mancini et al. (2020).

3.1 System Parameters

General properties of the scale-model wind turbine are given in Table 1 and Table 2. The general configuration is shown in Figure 3. While the system has the ability to apply active control, the tests considered in this project only include steady conditions with fixed rotor speed and blade pitch angle. Also, because the inertial loads are subtracted out of the force measurements, no mass or inertia values for the structure are provided. If they are needed, participants are welcome to enter a dummy value of their choice.

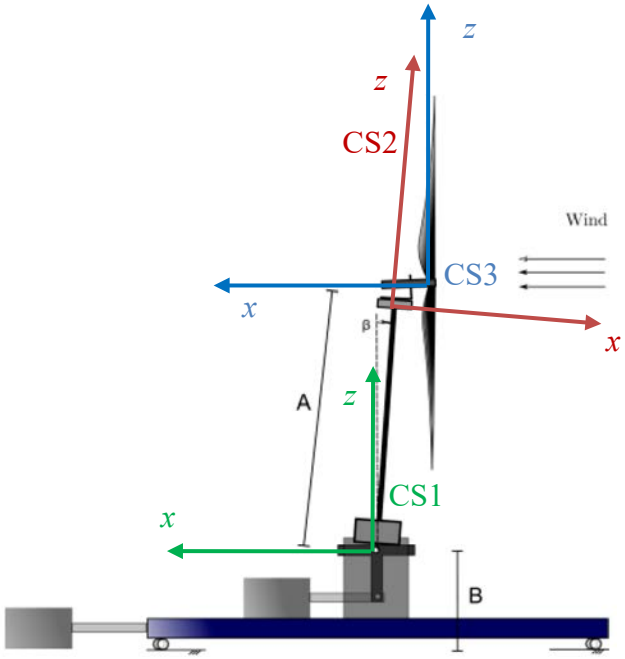

Figure 3. Test setup during the UNAFLOW project in the Polimi wind tunnel.

The rotor is vertical due to offsetting tower pitch and shaft tilt, but tower-top force measurements are offset by 5 deg (coordinate system 2 (CS2); located at [A × cos(β) + B] above ground). Displacements are measured in the inertial reference frame (CS1; x-axis parallel to the ground). PIV measurements are made relative to CS3, whose origin is at the hub center. β is a constant imposed pitch angle of tower/turbine (5 deg).

Table 1. Key Properties of the Polimi Model Turbine

Parameter	Value
Configuration	Three-bladed, clockwise upwind rotation
Control	Variable speed + individual pitch
Drivetrain	Transmission belt, epicyclic gearbox
Gearbox Ratio	42

Both testing campaigns were performed with the same rotor (i.e., blades and hub). However, the rotor overhang distance, the tower length, and the distance from the wind tunnel floor to the tower base are different. This results in a slight difference in the hub height between test campaigns.

Table 2. Polimi Turbine Model Configuration

Parameter	Model Value UNAFLOW	Model Value Follow-on Campaign
Rotor Diameter	2.38132 m	
Blade Length	1.10166 m	
Hub Height	2.086 m	2.188 m
Hub Diameter	0.178 m	
Rotor Overhang[a]	0.09467 m	0.139 m
Tilt Angle	5 deg	
Coning Angle	0 deg	
Blade Prebend	0 m	
Twr2Shft[b]	0.03667 m	0.064 m
Tower Diameter	0.075 m	
Tower Length	1.6057 m	1.400 m
Tower Base Offset	0.450 m	0.730 m

[a] Overhang = distance from yaw axis to rotor apex (along *x*-axis in CS3)

[b] Twr2Shft = distance from tower-top to the rotor shaft (along *z*-axis in CS2)

3.2 Blades

The airfoils used for the scaled turbine are a 10% thick version of the Selig Database SD7032 airfoil, which is a low-Reynolds-number airfoil that achieves good characteristics with Reynolds numbers in the range of 100,000–200,000. Developing a scaled rotor that can accurately represent all phenomena correctly is difficult, and thus the blades in the rotor were built to be rigid to eliminate the difficulty in scaling the aeroelastic behavior. Separate two-dimensional (2D) testing was performed to characterize the airfoils used in the scaled experimental campaign (Fontanella et al. 2021). The airfoil polars were developed from these 2D tests (which can feed lifting line codes). The lift coefficients are obtained from pressure taps at the model midspan, and the drag coefficients are obtained from a wake rake.

Polars for the model-scale blades are provided at 20 radial stations, as summarized in the ***airfoil_data.mat*** file (In case MATLAB is not available, Appendix A.2 provides a script to read this data in Python). This MATLAB file contains a three-dimensional (3D) array of size 128 × 15 × 20. The 15 columns correspond to the angle of attack in degrees and seven sets of lift and drag coefficients for Reynolds numbers of 5.0E4, 6.0E4, 7.5E4, 1.0E5, 1.5E5, 1.7E5, and 2.0E5. The third dimension corresponds to the 20 radial stations from blade root to blade tip, as stated in Table 3. Figure 4 shows one schematic representation of the 3D array containing this information.

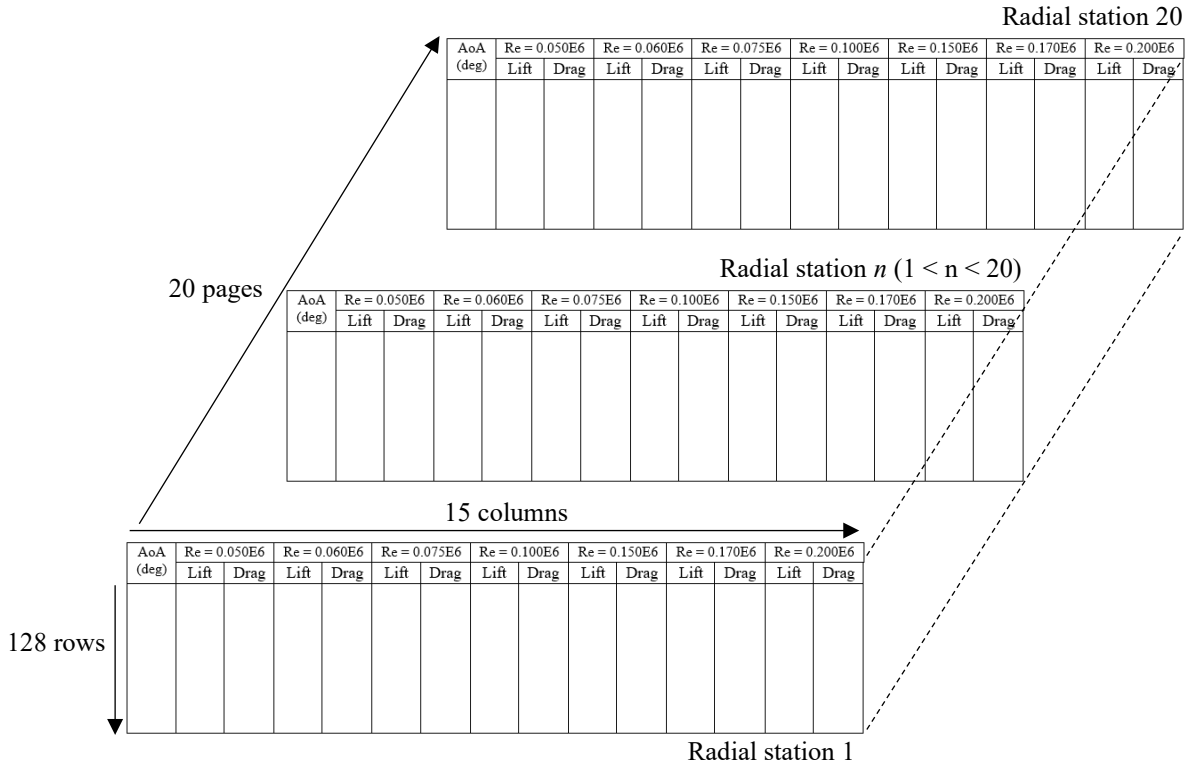

Figure 4. Schematic representation of the *airfoil_data.mat* 3D array.

AoA = angle of attack; Re = Reynolds number

For reference, Figure 5 shows the lift and drag coefficients according to the angle of attack for radial station 10 when the Reynolds number is equal to 1.0E5.

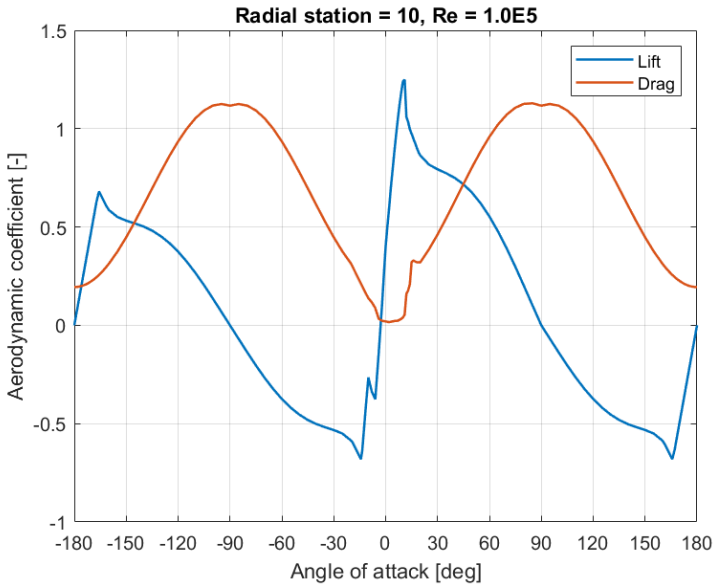

Figure 5. Aerodynamic coefficients for the radial station 10 when the Reynolds number is equal to 1.0E5

The postprocessing of the 2D measurements consisted of (1) the SD7032 polars for the different Reynolds numbers were extrapolated to the −180/+180 angle of attack range by means of the Viterna method; (2) the polars for the transition sections, where the airfoil gradually passes from the circular section to the SD7032, were obtained by means of linear interpolation; and (3) the 3D corrections were applied to the polars of the single radial stations. Stall-delay corrections were applied for a single radial station at a time based on methodologies from Du and Selig (1998) and Eggers, Chaney, and Digumarthi (2003). For blade stations with $r/R < 0.35$, the 3D corrections were the same as for those with $r/R = 0.35$. The tip speed ratio was modified according to the Du–Selig stall-delay method (Du and Selig 1998).

It is important to realize that the polars provided in the ***airfoil_data.mat*** file already contain the rotational augmentation corrections for 3D delayed stall. Some simulation tools have this capability built in. To avoid double-counting for these corrections, the participant should disable this option in the simulation tool. In case this is not possible, the participant should use the raw data from the measurements (***UNAFLOW_turb_polars.mat***). These measurements correspond to the airfoil with relative thickness of 9.97% and the Reynolds numbers of interest. The angles of attack measured (from −10 to +25 deg) will have to be extrapolated to the whole range (e.g., from −180 to +180 deg) by means of the Viterna method. For the lift coefficients, an angle of attack of +14 deg, and for the drag coefficients an angle of +20 deg were used instead of the +25 deg to apply the Viterna method. The participant can also take advantage of the circular section (relative thickness = 100%) defined in ***airfoil_data.mat*** to allow the simulation tool to interpolate the intermediate relative thickness between 100% and 9.97%.

The blade aerodynamic properties, including chord-twist-thickness-pitch axis-airfoil type, are available in Table 3. The aerodynamic twist angle follows the same convention as the blade pitch angle (i.e., positive to feather, leading edge upwind). The aerodynamic center of the different radial stations is coincident with the blade pitch axis (see Figure 6). A computer-aided design model of the blade 3D geometry is also available: ***palaDev1_Final_mm.igs***.

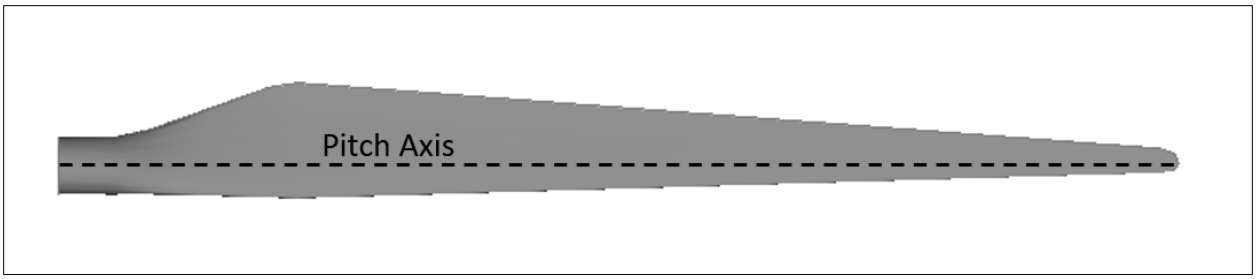

Figure 6. 3D geometry from *palaDev1_Final_mm.igs* with the pitch axis

Table 3. Distributed Blade Properties

Radial Station	Percent span from the centerline[a] (%)	Distance along pitch axis from blade root (m)	Chord (m)	Aerodynamic twist (deg)	Aerodynamic center (% chord)	Relative thickness (%)	Airfoil ID[b] (-)
1	7.5	0.00000	0.05585	17.07668	50.00	100.00	2
2	12.4	0.05817	0.05678	17.04199	48.76	75.88	3
3	18.9	0.13641	0.07573	15.77593	35.76	17.91	5
4	25.8	0.21766	0.10620	12.30509	29.08	11.11	7
5	32.7	0.30059	0.11490	9.98299	29.00	9.97	9
6	39.7	0.38379	0.11044	8.65143	29.00	9.97	11
7	46.6	0.46581	0.10236	7.56522	29.00	9.97	13
8	53.3	0.54530	0.09272	6.38165	29.00	9.97	15
9	59.6	0.62105	0.08288	5.08008	29.00	9.97	17
10	65.6	0.69211	0.07356	3.79042	29.00	9.97	19
11	71.1	0.75778	0.06516	2.61685	29.00	9.97	21
12	76.1	0.81765	0.05778	1.59090	29.00	9.97	23
13	80.7	0.87153	0.05141	0.71754	29.00	9.97	25
14	84.7	0.91947	0.04604	0.03751	29.00	9.97	27
15	88.2	0.96171	0.04163	-0.53510	29.00	9.97	29
16	91.3	0.99860	0.03796	-1.03393	29.00	9.97	31
17	94.0	1.03056	0.03440	-1.46251	29.00	9.97	33
18	96.3	1.05807	0.03054	-1.61172	29.00	9.97	35
19	98.3	1.08162	0.02541	-1.60710	29.00	9.97	37
20	100.0	1.10166	0.00998	-1.72236	29.00	9.97	39

[a] Underlined values denote the radial stations where local aerodynamic quantities are requested for verification purposes (see section 6.2).

[b] Previous studies from Polimi considered 39 radial stations with 39 unique airfoils. OC6 Phase III project simplified the definition to 20 radial stations.

Figure 7 shows the chord and aerodynamic twist variation along the blade according to Table 3.

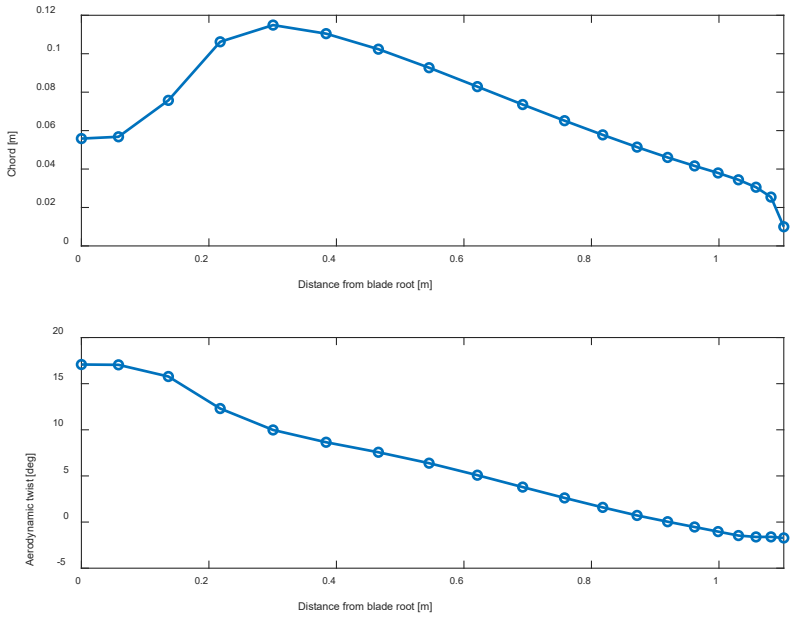

Figure 7. Chord and aerodynamic twist along the blade

Table 4 shows the Reynolds numbers used at each radial station along the blade for the load cases proposed in Section 5. These data are aligned with the work done by Fontanella et al. (2021). This table can be useful for the participants using a simulation tool that does not interpolate between airfoils according to the Reynolds number. In case more than one airfoil is used (e.g., in the radial stations from 4 to 19), the participant can calculate the corresponding Reynolds number for the load case of interest. Equation 1 shows the Reynolds number calculation.

$$R_e = \frac{uL}{v} \tag{1}$$

where u is the flow speed (i.e., relative wind speed) in meters per second, L is the characteristic length (e.g., the chord) in meters, and v is the kinematic air viscosity (e.g., 1.460E-05 m^2/s).

Table 4. Reynolds Numbers Necessary (Highlighted in Gray)

Radial Station	5.0E+04	6.0E+04	7.5E+04	1.0E+05	1.5E+05	1.7E+05	2.0E+05
1							
2							
3							
4							
5							
6							
7							
8							
9							
10							
11							
12							
13							
14							
15							
16							
17							
18							
19							
20							

3.3 Rotor Nacelle Assembly

The rotor has a tilt of 5 deg (but it is negated by the tower pitch offset). The overall mass and inertia properties of the rotor nacelle assembly are not provided, as the inertia effects have been removed from the measurements. Modelers may specify their own mass/inertia properties if needed (e.g., mass = 1 kg), but then the associated inertia effects will need to be removed from the simulation results.

Computer-aided design models are available for the hub (***Nose.stp***) and the nacelle assembly (***NacelleAssembly.stl***).

3.4 Tower

The tower was built to be rigid to avoid issues with measurements. A constant pitch offset (5 deg) was applied to have the rotor perpendicular to the wind tunnel floor, effectively negating the turbine tilt angle. The tower diameter is 75 millimeters (mm). The tower shadow effect results in a three-per revolution (3P) excitation over the system and the corresponding harmonics. Appendix A.7 shows a sensitivity analysis of the tower influence in OpenFAST.

4 Wind Tunnel Blockage

The presence of the scaled wind turbine in the test section reduces the flow area compared to an undisturbed and unrestricted freestream. This flow area reduction increases the wind velocity. According to Polimi, the inflow wind was measured 7.15 m upstream, and the induction influence at that location can be considered negligible. The blockage ratio (ε) between the rotor disk cross-area (A_d) and the wind tunnel cross area (C) can be calculated according to Equation 2:

$$\varepsilon = \frac{A_d}{C} = \frac{\pi * \left(\frac{2.38132}{2}\right)^2}{13.84 * 3.84} = 0.084 \quad (2)$$

According to the correction methodology for blockage in wind tunnels developed by Glauert (1936), the wind in unconfined conditions (U'_∞) can be related to the wind in confined conditions (U_∞) according to Equation 3:

$$\frac{U'_\infty}{U_\infty} = 1 + \varepsilon \frac{C_T}{4\sqrt{1 - C_T}} \quad (3)$$

where the thrust coefficient (C_T) is given by Equation 4:

$$C_T = \frac{T}{\frac{1}{2}\rho A_d U_\infty^2} \quad (4)$$

where T is the measured thrust force in newtons and ρ is the air density (1.177 kg/m^3).

5 Load Cases

5.1 Load Case 1.X – Steady Wind

During the UNAFLOW project, the turbine was tested in a fixed condition with three different wind speeds (U_∞): two rated cases (Rated 1 and 2) and one above-rated case. The rated cases were carried out with a steady rotational speed (Ω; in revolutions per minute [rpm]) corresponding to an optimal tip-speed ratio (Λ), and with the blades in a neutral position. For the above-rated case, the blades were collectively pitched (θ_P) to 12.5 deg. The Rated 1 condition at 2.5 m/s will not be considered in this validation project, as the signal-to-noise ratio for this wind speed was not as good as for Rated 2. The follow-on test campaign carried out by Polimi was also focused on the Rated 2 and the above-rated conditions. The steady-wind load cases performed are summarized in Table 5.

Table 5. Load Case 1.X Prescription

Load Case	U_∞ (m/s)	U'_∞ (m/s)	Ω (rpm)	Λ (-)	θ_P (deg)
1.1 – Rated 2	4.00	4.19	240	7.1	0
1.2 – Above Rated	6.00	6.03	265	5.5	12.5

The wind speeds in Table 5 show both the wind speeds measured upstream and not impacted by the presence of the scaled wind turbine (U_∞) and the wind speed corrected due to the wind tunnel blockage (U'_∞). The corrected wind speed values were obtained by evaluating Equation 3. Figure 8 shows the wind tunnel blockage correction that should be applied according to the thrust coefficient.

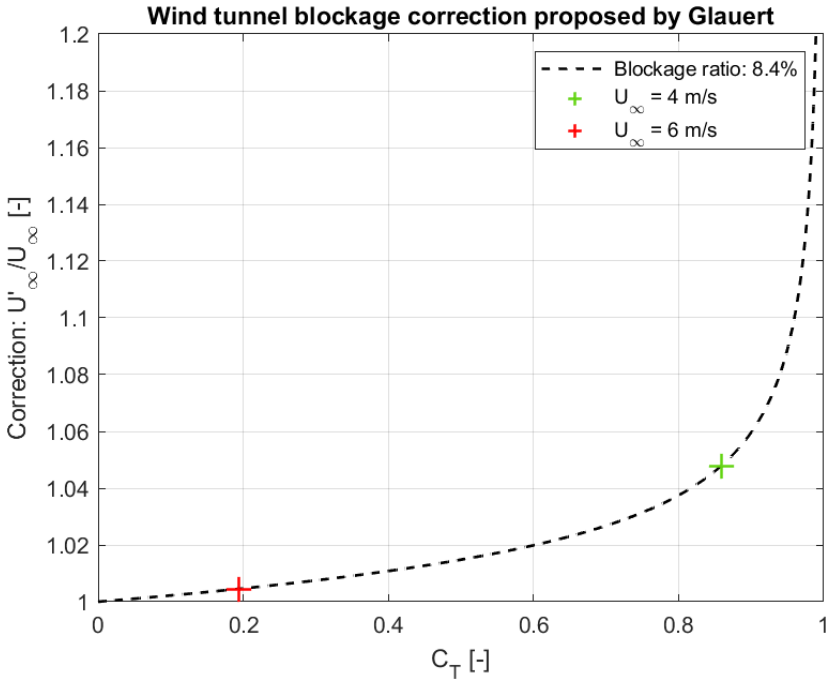

Figure 8. Wind tunnel blockage correction

5.2 Load Case 2.X – Unsteady Wind

For the unsteady wind cases, the wind turbine system was forced to oscillate in the surge direction using varying frequencies (F) and amplitudes (A) under the same wind conditions as the fixed condition (e.g., LC 1.X). Surge motion has one of the largest amplitudes of motion for a floating platform. The amplitude was limited for certain frequencies to ensure dynamic stall was confined to the blade root (see Fontanella et al. [2021] for more information). A summary of the load cases for LC 2.X is given in Table 6. Four load cases shaded in this table should be prioritized for high-fidelity simulations where it is not practical to run all simulations. LC 2.1, LC 2.5, and LC 2.7 will be the ones used to analyze the wake. A full list of oscillation cases performed during the UNAFLOW campaign is given in the Appendix (Appendix A.4). LC 2.1, LC 2.5, and LC 2.7 were also tested during the follow-on campaign (see Appendix A.5). One additional load case (LC 2.12) has been added for verification purposes. The goal is to try to increase the influence of the dynamic inflow with wind speed variations around 25% of the inflow wind. This wind speed variation is around 4.5 times higher than the largest value considered during the experiment in LC 2.5.

Each load case was simulated for enough time to assess the average, steady-state condition. One will need to consider the time to eliminate any initial transient responses.

Table 6. Load Case 2.X Prescription

Load Case[a]	U'_∞ (m/s)	F_{surge} (Hz)	A_{surge} (m)	Ω (rpm)	θ_P (deg)	CW[b]	AW[c]	PIV	Test No.
2.1	4.19	0.125	0.125	240	0	✓	✓	✓	33
2.2	4.19	0.125	0.03	240	0	✓		✓	36
2.3	4.19	0.5	0.065	240	0	✓	✓	✓	41
2.4	4.19	0.5	0.015	240	0	✓		✓	44
2.5	4.19	1.0	0.035	240	0	✓	✓	✓	50
2.6	4.19	1.0	0.01	240	0	✓		✓	52
2.7	4.19	2.0	0.008	240	0	✓	✓	✓	59
2.8	4.19	2.0	0.004	240	0	✓		✓	60
2.9	6.03	0.125	0.125	265	12.5	✓		✓	65
2.10	6.03	1.0	0.035	265	12.5			✓	83
2.11	6.03	2.0	0.0125	265	12.5	✓		✓	91
2.12	4.19	2.0	0.080	240	0	✓	✓		NA

[a] Note: only LC 2.1, LC 2.5, LC 2.7, and LC 2.12 (shaded) were studied by the participants in the project.

[b] CW: cross-wind hot-wire measurements.

[c] AW: along-wind hot-wire measurements.

During platform motion, the wind turbine rotor loads (e.g., thrust and torque) will be impacted, likely resulting in a rotor speed variation and/or blade pitch actuation. Two new load cases, LC

2.16 and LC 2.17, were proposed to study the system behavior. These additional load cases are based on LC 2.12. LC 2.16 includes rotor speed variations that are on the order of 15% with respect to the rotor speed in steady conditions. This load case can be considered representative of the wind turbine operating below rated conditions. LC 2.17 includes blade pitch actuations. The blade pitch angle oscillates between 0 and 3 deg with an average value of 1.5 deg. This load case can be considered representative of the wind turbine operating above rated conditions. See Table 7 for reference.

Table 7. Load Case 2.X With Rotor Speed and Blade Pitch Variations

Load Case	U'_∞ (m/s)	F_{surge} (Hz)	A_{surge} (m)	Ω (rpm)	θ_P (deg)	CW	AW	PIV	Test No.
2.16	4.19	2.0	0.080	240±36	0	✓	✓		NA
2.17	4.19	2.0	0.080	240	1.5±1.5	✓	✓		NA

The rotor speed and blade pitch variations presented in Table 7 follow the apparent wind that results from the free inflow wind and the surge platform motion. The surge motion describes a negative sine function while the rotor speed and blade pitch angle follow a positive cosine function. Figure 9 illustrates the platform surge motion and the corresponding rotor speed and blade pitch variations.

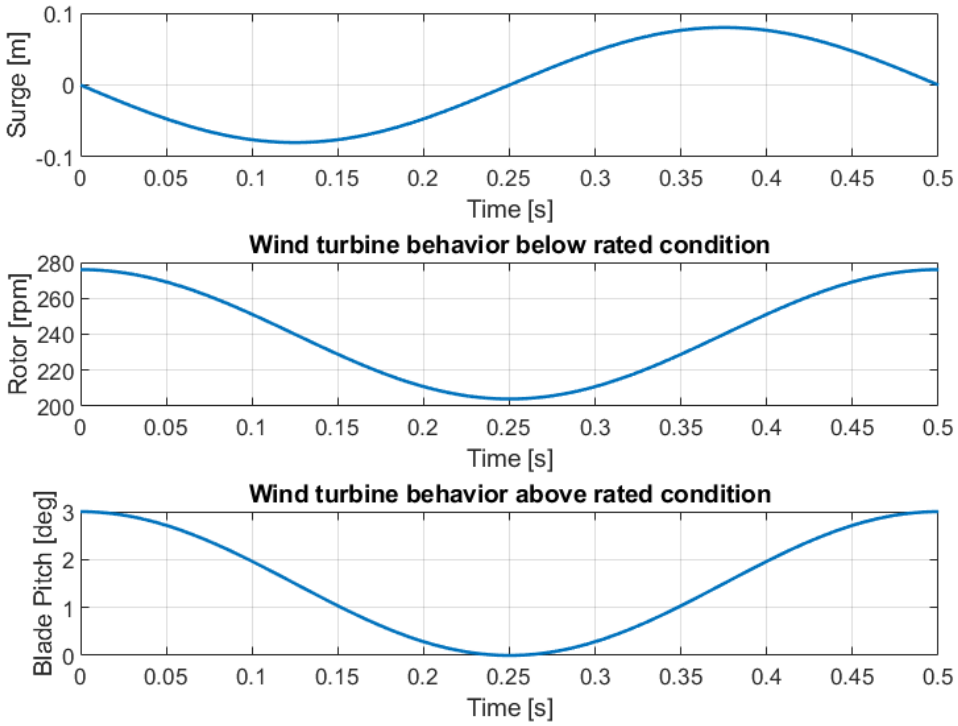

Figure 9. Platform surge motion (top), rotor speed variation in LC 2.16 (middle), and blade pitch variation in LC 2.17 (bottom) during one surge period

When the platform moves in the negative surge direction (i.e., upwind) and it is at its maximum speed (e.g., when passing through surge = 0 m at time t = 0 seconds [s] and t = 0.5 s), the rotor experiences the highest apparent wind. This higher wind results in higher loads that will speed up

the rotor when the wind turbine is working below rated speed conditions or will trigger the blade pitch actuation to avoid overspeed when the wind turbine is working above rated conditions. In this case, it is assumed that the system reacts instantaneously (e.g., there are no system dynamics involved).

5.3 Load Case 3.X – Unsteady Wind

The wind turbine system was forced to oscillate in the pitch direction using varying frequencies and amplitudes under the same wind conditions as the fixed condition (e.g., LC 1.X). Moreover, the platform pitch motion was prescribed in a way that it results in the same reduced frequencies and apparent wind for the rotor as the ones studied for the surge motion. The only load case that does not satisfy this condition is LC 3.1 due to a limitation with the maximum platform pitch amplitude allowed by the robot (3 deg). A summary of the load cases for LC 3.X is given in Table 8. For this testing campaign, only the loads were measured. There are no hot-wire or PIV measurements. A full list of oscillation pitch cases performed is given in Appendix A.6.

Table 8. Load Case 3.X Prescription

Load Case	U'_∞ (m/s)	F_{pitch} (Hz)	A_{pitch} (deg)	Ω (rpm)	θ_P (deg)	CW	AW
3.1	4.19	0.125	3.000	240	0	✓	✓
3.5	4.19	1.0	1.400	240	0	✓	✓
3.7	4.19	2.0	0.300	240	0	✓	✓

6 Outputs

For each load case, five sets of text files were generated for the results, which are summarized in the following subsections. These include outputs related to the forces, blade aerodynamics, and wake measurements. A summary of output files is shown in Table 9.

Table 9. Summary of Output Files

Output Type	Load Cases	Total No. Files
Forces	All load cases (1.X, 2.X, and 3.X)	11
Blade Aerodynamic Response	All load cases (1.X, 2.X, and 3.X)	11
Hot-Wire	1.1, 1.2, 2.1, 2.5, 2.7, 2.12, 2.16, 2.17, 3.1, 3.5, 3.7	22
PIV – Steady	1.1, 1.2	34
PIV – Unsteady	2.1, 2.5, 2.7, 3.1, 3.5, 3.7	210

6.1 Force Output Files

The first output file is focused on reporting the 6-degrees-of-freedom force magnitudes (*Fx*, *Fy*, *Fz*, *Mx*, *My*, *Mz*) at the hub (CS3 in Figure 3). An output time step of 0.025 s was used. Each file should contain eight columns with outputs described in Table 10. The first line should be a header line or should be kept blank. The columns must be delimited by tab-separated or space-separated values.

Simulation outputs for LC 1.X should include only one line of data for the steady-state condition (averaged over one rotor revolution). For columns 1 and 2, the participant can write "0" or "NaN" (i.e., not a number). If some outputs are not available, the participant can write "NaN" so the rest of the available data can be postprocessed. For LC 2.X or LC 3.X, simulation outputs should include one full period of a surge or pitch oscillation. The surge displacement should start at 0 m, and then be decreasing, creating a negative sine function. The platform pitch displacement should start at 0 deg (tower is rotated −5 deg under that condition) and then increase, creating a positive sine function. In case the response is not periodic, the outputs reported by the participant should represent an averaged output over multiple periods. The mass/inertia/gravity components should be removed from the reported forces/moments.

For the sake of simplicity, it was requested that the platform surge motion follows a negative sine function (e.g., the platform starts moving in the upwind direction) to be aligned with the sequence on how the PIV measurements were recorded (described in Section 6.4). This platform motion is opposite to the one described during the platform pitch testing. If participants would start reporting the outputs when the platform starts moving downwind, they would be forced to report 1.5 periods to cover the load and PIV measurements (see Figure 10 for reference).

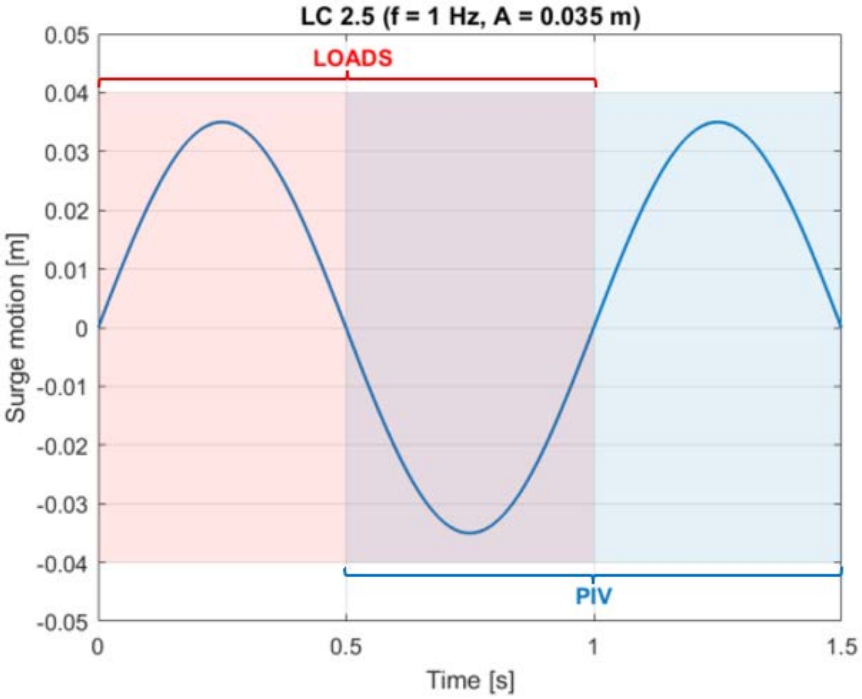

Figure 10. Loads and PIV outputs are requested for a surge motion that describes a negative sine function for simplicity

NREL processed the loads provided by the participants during the platform surge motion, applying a 180-deg phase shift to the loads. Therefore, the results will be equivalent to the platform moving in the downwind direction at $t = 0$ s. Like this, the loads can be directly compared to the pitch tests that describe a positive sine function (e.g., platform moving in the downwind direction at $t = 0$ s).

The total number of rows in the output file will differ for LC 2.X and LC 3.X, as the total simulation time will be different based on the period of the surge/pitch oscillations. One output file should be generated for each load case, for a total of 11 output files.

Table 10. Force Results Output Format

Column Number	Output	Units
1	Time	s
2	*x*-displacement or *y*-rotation	m or deg
3	*Fx* – Hub	N
4	*Fy* – Hub	N
5	*Fz* – Hub	N
6	*Mx* – Hub	N·m
7	*My* – Hub	N·m
8	*Mz* - Hub	N·m

The naming convention for each file should include the institution's name submitting the results, followed by the modeling approach, and type of output. As an example, for the force output file in LC 1.1, NREL's file would be named:

NREL_M12_LC11_Forces.txt

The two numbers after "M" refer to the modeling approach. The first number (1–5) will be based on which of the wake/induction modeling approaches listed below are used, and the second number (1–4) will provide information about the blade/airfoil model used. So, this file indicates a blade/element momentum (BEM) approach with a blade/airfoil model that accounts for a lifting line with static polars.

Participants submitting results filled out more information on their modeling approach for a better understanding of the comparison between participant results. Appendix A.3 provides further details for the wake/induction and blade/airfoil models that were provided.

Wake/Induction Model

1. Blade element/momentum (BEM)
2. Dynamic (filtered) blade element/momentum (DBEM)
3. Generalized dynamic wake (GDW)
4. Free vortex-wake (FVW)
5. Computational fluid dynamics (CFD).

Blade/Airfoil Model

1. Disk (thrust/torque)
2. Lifting line with static polars
3. Lifting line with unsteady airfoil aerodynamics
4. Blade resolved/surface mesh.

6.2 Blade Aerodynamic Response

For all load cases, local aerodynamic quantities along the blade were reported. Though there were not measurements taken of these loads, they will be useful to help understand differences in the loads/wake between simulation models. After the time column, the results are organized in six groups of nine columns each—including (1) the normal force per unit length (normal to the rotor plane, positive along the wind direction), (2) the tangential force per unit length (tangential to the rotor plane, positive in the direction of rotation), (3) the relative wind speed (including inflow wind, rotor rotation, and induction), (4) the angle of attack, (5) the lift coefficient, and (6) the drag coefficient—as summarized in Table 11. Within each group, the local aerodynamic quantities should be provided for nine radial stations, starting at 18.9% span and going to 98.3% span, skipping every other station—underlined in Table 3. The local aerodynamic quantities should be obtained by averaging across the three blades. The file formatting should follow that of

the force output files, including the time step, number of rows, and naming convention (using "BA" for "blade aerodynamics"). The results file should be labeled following this example:

NREL_ M12_LC11_BA.txt

Table 11. Blade Aerodynamic Results Output Format

Column Number	Output	Units
1	Time	s
2–10	Normal force (to plane)	N/m
11–19	Tangential force (to plane)	N/m
20–28	Relative wind speed	m/s
29–37	Angle of attack	deg
38–46	Lift coefficient	(-)
47–55	Drag coefficient	(-)

6.3 Hot-Wire Probe Measurements

A hot-wire probe was set up to measure all three wind components (u, v, and w). Measurements were taken while the probe traversed the cross-wind direction (y) and along-wind direction (x), following CS3. For the cross-wind motion (see Figure 11, left), the probe started at the hub location, but 2.3 diameter (D) downstream (5.48 m), and moved from −1.6 m to 1.6 m in the y-direction with a spatial discretization of 100 mm (33 points). For the along-wind motion, the probe started with a 0.9 m offset in the y-direction and moved between 0.9 and 2.3D (2.18–5.48 m) in the x-direction, with a discretization of 330 mm (11 points). Figure 12 shows the wind turbine rotor as well as the PIV vertical plane (detailed in Section 6.4) and the hot-wire measurement points for the along-wind and cross-wind directions.

Measurements as outlined in Table 12 were provided for load cases LC 1.X, LC 2.X, and LC 3.X. For each load case, one cross-wind (CW) and one along-wind (AW) file will be created, for a total of 22 files. Note, the probe x-location will be a set value of 5.48 m for the cross-wind files, whereas the probe y-location will be a set value of 0.9 m for the along-wind files. Like Sections 6.1 and 6.2, the results should be provided for one oscillation cycle. For the surge motion, this means starting at surge amplitude of 0 m and move in the negative x-direction, creating a negative sine function. For the pitch motion, this means starting at pitch amplitude of 0 deg (tower effectively tilted −5 deg) and rotate around the y-axis, creating a positive sine function. The time step used to report the outputs should be 0.025 s. The output files containing the along-wind and cross-wind results should be labeled following this example:

NREL_ M12_ LC21_HW_AW.txt, NREL_ M12_ LC21_HW_CW.txt

Table 12. Hot-Wire File Output Channel List (Relative to CS3)

Column Number	Output	Units
1	Time	s
2	*x*-displacement	m
3	Probe *x*-location	m
4	Probe *y*-location	m
5	*u*-velocity (*x*-dir)	m/s
6	*v*-velocity (*y*-dir)	m/s
7	*w*-velocity (*z*-dir)	m/s

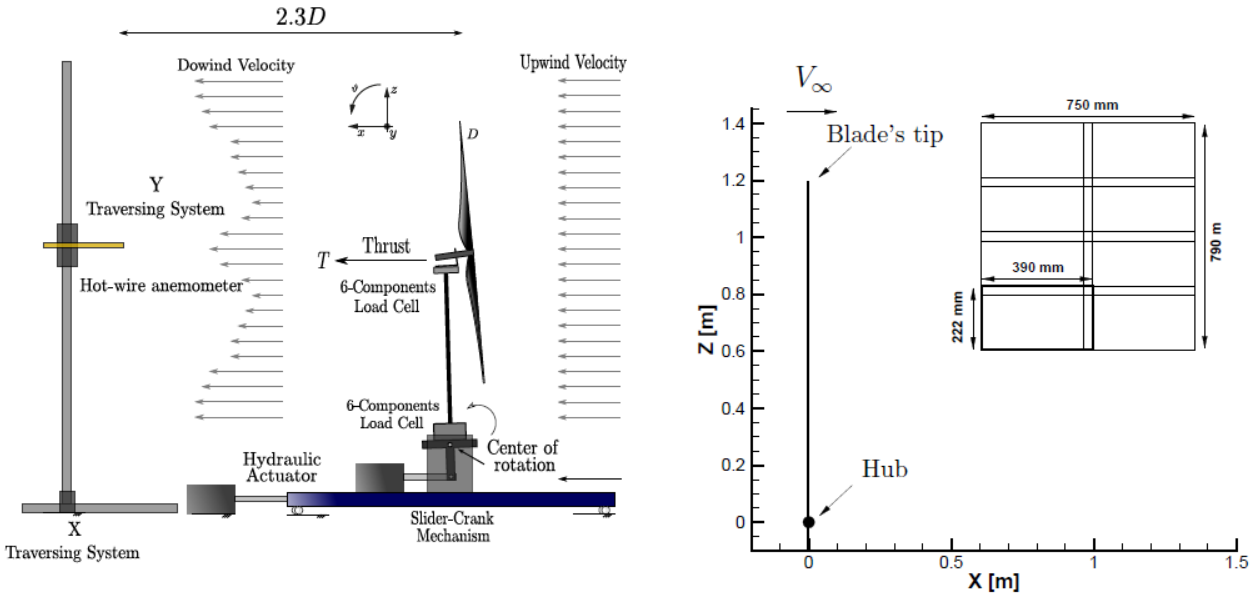

Figure 11. Measurement information for hot-wire (left) and PIV (right). Note: turbine not in correct orientation in this picture (Bayati et al. 2018)

6.4 PIV Steady Wind Output Files (Load Case 1.X)

For the PIV measurements, two sets of output files were generated, one for steady conditions and another for unsteady. The general format is shown in Table 13. Again, the first line of all files can be a header line (optional).

Table 13. PIV File Output Channel List

Column Number	Output	Units
1	*x*-location	m
2	*z*-location	m
3	*u*-velocity (*x*-dir)	m/s
4	*w*-velocity (*z*-dir)	m/s
5	Vorticity magnitude (ω; about *y*-dir)	1/s

For LC 1.X, a file was output at each of the azimuth angles $\psi = 0$ deg to $\psi = 120$ deg with a 15-deg step, and from $\psi = 120$ deg to $\psi = 360$ deg with a 30-deg step (17 total azimuth angles). Each file reports wind speeds at locations equal to $x = 0.61$ m and increasing to 1.36 m with 5-mm increments, and $z = 0.61$ m to 1.4 m with 5-mm increments (24,009 lines + 1 header line). Note, the first point should be $x = 0.61$, $z = 0.61$, then increase x values incrementally while holding z fixed. Then, increment z and repeat. The CS3 coordinate system (see Figure 3) should be used, which has the origin at the hub center. Figure 12 shows the location of the PIV plane behind the rotor as well as the location of the hot-wire measurements. For each of the two load cases (LC1.1 and LC1.2), 17 files will be generated. The example naming is as follows:

NREL_M43_LC11_PIV_PSI0.txt, NREL_M43_LC11_PIV_PSI15.txt, ...

meaning that these files contain PIV measurements for LC 1.1 at 0 deg and 15 deg azimuth angle.

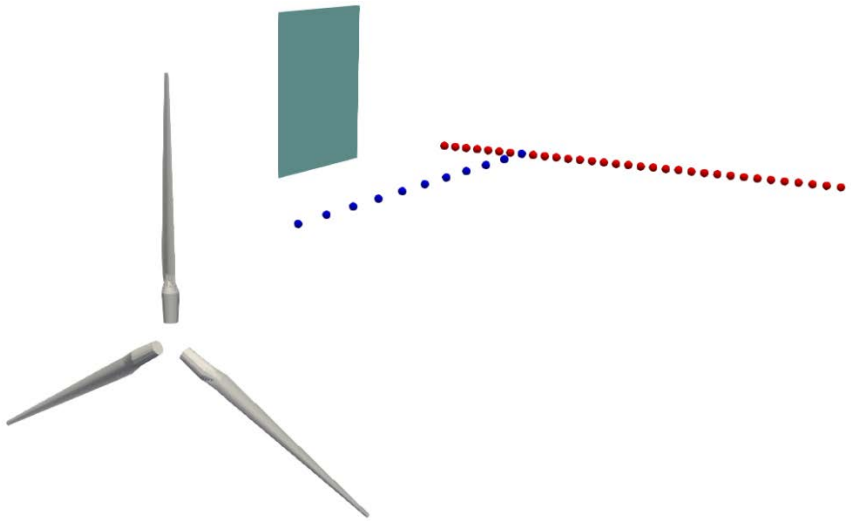

Figure 12. Wind turbine rotor, PIV measurement (green plane), hot-wire along-wind direction (blue dots), and hot-wire cross-wind direction (red dots)

6.5 PIV Outputs for Unsteady Wind (Load Case 2.X and Load Case 3.X)

For LC 2.X and LC 3.X, the PIV measurements at two rotor azimuth positions shall be outputted at distinct locations in the surge or pitch oscillation cycle. LC 2.X and LC 3.X have a rotor rotational frequency (1P) of 4 Hz, which is a multiple of the surge and pitch frequencies. Thus, the same azimuth position will occur at evenly spaced positions in the surge or pitch oscillation. As an example, LC 2.1 and LC 3.1 have a 0.125-Hz surge/pitch frequency, so there will be 32 evenly spaced instants (4 Hz/0.125 Hz) where the same azimuth angle will occur (e.g., at 0 s, 1/P s, 2/P s, 3/P s, …). See Figure 13 for reference. Unfortunately, for LC 2.5 or LC 3.5 the surge or pitch frequency is 1 Hz and there are only four locations where the same azimuth angle will occur. The same limitation occurs for LC 2.7 and LC 3.7, where there are only two locations during the platform motion with the same azimuth angle. To improve the postprocessing of these results, the outputs from the numerical models are requested every 60 deg in azimuth in LC 2.5, LC 2.7, LC 3.5, and LC 3.7.

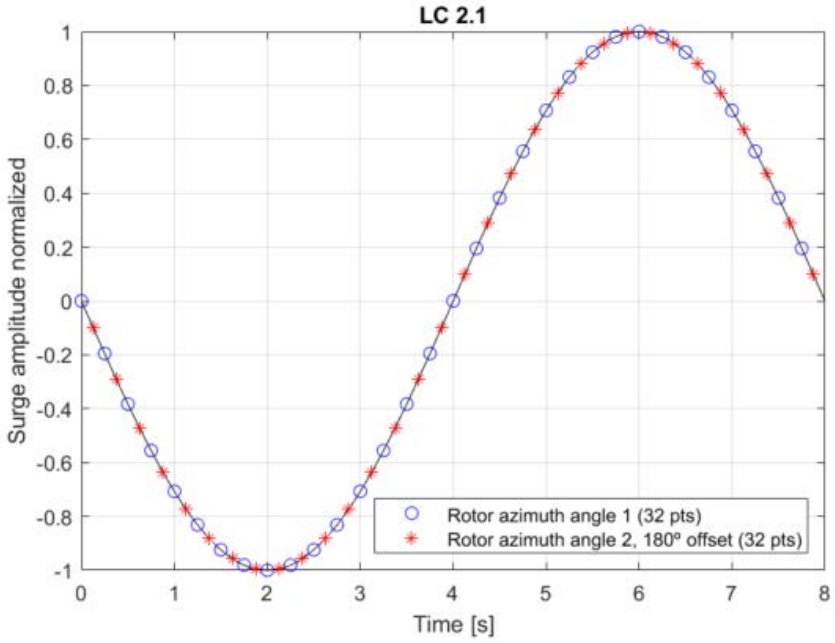

Figure 13. 64 instants during one surge period to report the PIV results in LC 2.1

As summarized in Table 14, PIV measurements were obtained at two different azimuth locations (180 deg offset) in LC 2.1 and LC 3.1, so a total of 64 instants (Steps 1–64) are requested. In LC 2.5 and LC 3.5, the PIV outputs are requested for a total of 24 instants (Steps 1–24) every 60 deg azimuth. Similarly, in LC 2.7 and LC 3.7 the outputs are requested for a total of 12 instants (Steps 1–12). The values reported should be for a single cycle after the initial transient response has died out.

The naming convention is shown in the example below. The files should contain the outputs designated in Table 14. The contents of the file should have the same format as was summarized for the steady-wind files in Section 6.4.

NREL_M43_ LC21_PIV_ STEP1.txt, NREL_M43_LC21_PIV_ STEP2.txt, …

Table 14. Details for PIV Output During One Platform Period

Load Case	Surge or Pitch Frequency (Hz)	Rotation Frequency (Hz)	Rotor Azimuth Positions (deg)	Number Translation or Rotation Locations	Time Discretization (s)
2.1 and 3.1	0.125	4.0	49, 229	64	T/64
2.5 and 3.5	1	4.0	7, 187	24	(T/8)/3
2.7 and 3.7	2	4.0	48, 228	12	(T/4)/3

7 Validation Method

7.1 Validation Objective

The objective of the validation campaign was to assess the ability of aerodynamic modeling approaches to accurately capture the loads and wake behavior on a wind turbine when in an unsteady condition created by large motion of the turbine.

7.2 Validation Quantities of Interest

The quantities of interest to assess this objective were:

- Loads at the hub
- Turbine wake characteristics.

7.3 Validation Metrics

- F_x = Mean or instantaneous value of the aerodynamic thrust force at hub (N)
- ΔF_x = Amplitude of thrust variation (N)
- M_x = Mean or instantaneous value of the aerodynamic torque (M_x) at hub (N·m)
- ΔM_x = Amplitude of torque variation (N·m)
- φF_x = Phase difference between platform motion and aerodynamic thrust force (deg)
- φM_x = Phase difference between platform motion and aerodynamic torque (deg).

7.4 Uncertainty

No uncertainty information has been made available for these experimental campaigns. For future tests, some information may be available, including repeat testing.

References

Bak, C., F. Zahle, R. Bitsch, et al. 2013. *Description of the DTU 10-MW Reference Wind Turbine*. Roskilde: Technical University of Denmark. DTU Wind Energy ReportI0092.

Bayati, I., M. Belloli, L. Bernini, H. Giberti, and A. Zasso. 2017. "Scale Model Technology for Floating Offshore Wind Turbines." *IET Renewable Power Generation* 11(9): 1120–1126. https://doi.org/10.1049/iet-rpg.2016.0956.

Bayati I., L. Bernini, A. Zanotti, M. Belloli, A. Zasso. 2018. "Experimental Investigation of the Unsteady Aerodynamics of FOWT Through PIV and Hot-Wire Wake Measurements." *Journal of Physics: Conf. Series* 1037: 052024. DOI:10.1088/1742-6596/1037/5/052024.

Bernini, L., I. Bayati, D. Boldrin, M. Cormier, M. Caboni, and R. Mikkelsen. 2017. "UNsteady Aerodynamics for Floating Wind (UNAFLOW)." IRPWIND Report.

Cormier, M., M. Caboni, T. Lutz, K. Boorsma, and E. Kramer. 2018. "Numerical Analysis of Unsteady Aerodynamics of Floating Offshore Wind Turbines." *Journal of Physics: Conf. Series* 1037: 072048. DOI 10.1088/1742-6596/1037/7/072048.

Eggers, A., K. Chaney, and R. Digumarthi. 2003. "An Assessment of Approximate Modeling of Aerodynamic Loads on the UAE Rotor." 41st Aerospace Sciences Meeting and Exhibit, Jan. 6–9, 2003, Reno, NV. AIAA 2003-868.

Fontanella, A., I. Bayati, R. Mikkelsen, M. Belloli, and A. Zasso. 2021. "UNAFLOW: A Holistic Wind Tunnel Experiment About the Aerodynamic Response of Floating Wind Turbines Under Imposed Surge Motion." *Wind Energy Science* 6(5): 1169–1190.

Glauert, H. 1936. "Chapter IX - The experimental study of propellers." In *Division L of Aerodynamic Theory, Vol. IV*.

Mancini, S.; K. Boorsma, M. Caboni, M. Cormier, T. Lutz, P. Schito, and A. Zasso. 2020. "Characterization of the Unsteady Aerodynamic Response of a Floating Offshore Wind Turbine to Surge Motion." *Wind Energy Science* 5: 1713–1730.

Du, Zhaohui, and Michael Selig. 1998. "A 3-D Stall-Delay Model for Horizontal Axis Wind Turbine Performance Prediction." 1998 ASME Wind Energy Symposium, Jan. 12–15, 1998, Reno, NV. AIAA-98-0021.

Appendix A.

A.1 Measurement Descriptions

Table A-1. Output Data Format for Force Files in the UNAFLOW Campaign (PIV Separate)

Variable	Description	Type	Coordinate System
FTBxyz	Tower base force data from RUAG balance	Nacq rows – 6 columns scalar matrix	CS2[a]
FTBinfo	Tower base force info, data system of unit	String array	
FTTxyz	Tower top force data from ATI balance	Nacq rows – 6 columns scalar matrix	CS2
FTTinfo	Tower top force info, data system of unit	String array	
disp	Turbine displacement (mono harmonic	Nacq scalar array	CS1
dispInfo	filtered laser measurement)	String array	
fsamp	Turbine displacement info	Scalar	
fsampInfo	Acquisition frequency of the data	String	
t	Acquisition frequency info	Nacq scalar array	
tInfo	Acquisition time	String	

[a] The loads at the tower base are measured in a coordinate system parallel to CS2, but it has the opposite orientation (i.e., *z* axis points downwards and *x* axis points in the downwind direction).

The follow-on campaign only recorded the loads at the tower top location. The orientation is equivalent to the CS2, but *x*- and *y*-axes have the opposite orientation. The measurements in the follow-on campaign include the channels: *FTTxyz*, *FTTinfo*, *disp*, *dispInfo*, *fsamp*, *fsampInfo*, *t*, and *tInfo*.

A.2 Reading Blade Polars Data in Python

In case MATLAB or Octave software is not available, it is possible to read the blade polars data by means of the next lines of code in Python:

```
#Reading the *.mat file:
import scipy.io
mat = scipy.io.loadmat(r'C:\OC6_PhaseIII\airfoil_data.mat') #Point to your own path

#Getting 3-D array:
data = mat['airfoil_data']

#Getting the matrix for the radial station of interest:
radial_station = 1 #Define a value between 1 and 20
matrix_radial_station = data[:,:,radial_station-1]
```

A.3 Modeling Categorization

Tables A-2 and A-3 provide a categorization method for the modeling approach by participants. The main numbers are used in the labeling of the results. An example is given for the National Renewable Energy Laboratory (NREL) results.

Table A-2. Modeling Approach for Wake/Induction

	NREL_M12
1. Blade element/momentum (BEM)	X
a. Tip/root correction	X
b. High thrust correction	X
c. Skewed wake	X
d. Other	
2. Dynamic BEM	
a. Tip/root correction	
b. High thrust correction	
c. Skewed wake	
d. Other	
3. Generalized dynamic wake (GDW)	
4. Free vortex-wake (FVW)	
a. Vortex particle	
b. Vortex line	
i. Trailing vorticity - tip/root	
ii. Trailing vorticity - dist.	
iii. Trailing + shed vorticity	
c. Regularization	
d. Viscous diffusion	
e. Other	

5. Computational fluid dynamics (CFD)	
a. Reynolds-average Navier-Stoles (RANS)	
b. Large eddy simulation (LES)	
c. Detached eddy simulation (DES)	

Table A-3. Modeling Approach – Blade/Airfoil

	NREL_M12
1. Disk (thrust/torque)	
2. Lifting line w/ static polars	X
3. Lifting line, unsteady	
a. Øye	
b. Hansen, Gaunna, and Madsen (HGM)	
c. Beddoes-Leishman (BL)	
d. Other	
4. Blade resolved/surface mesh	

A.4 All Surge-Oscillation Tests Performed During the UNAFLOW Campaign

- U_∞: wind speed in the wind tunnel (confined conditions)
- F_{surge}: platform surge frequency
- A_{surge}: platform surge amplitude
- Vw: wake-reduced velocity

  $Vw = \frac{\frac{U_\infty}{F_{surge}}}{\emptyset}$ where $\emptyset$ is the rotor diameter
- Λ: tip-speed ratio
- Ω: rotor rotational speed
- θ_P: collective blade pitch angle
- CW: cross-wind hot-wire measurement
- AW: along-wind hot-wire measurement
- PIV: particle image velocimetry.

Table A-4. Surge Motion Tests (No Control)

Test #	U_∞ (m/s)	F_{surge} (Hz)	A_{surge} (m)	Vw	Λ	Ω (rpm)	θ_P	CW	AW	PIV
1	2.5	0.125	0.125	8.40	7.5	150	0			
2	2.5	0.125	0.12	8.40	7.5	150	0			
3	2.5	0.125	0.08	8.40	7.5	150	0			
4	2.5	0.125	0.04	8.40	7.5	150	0			
5	2.5	0.25	0.08	4.20	7.5	150	0			
6	2.5	0.25	0.06	4.20	7.5	150	0			
7	2.5	0.25	0.04	4.20	7.5	150	0			
8	2.5	0.25	0.02	4.20	7.5	150	0			
9	2.5	0.5	0.04	2.10	7.5	150	0			
10	2.5	0.5	0.03	2.10	7.5	150	0			
11	2.5	0.5	0.02	2.10	7.5	150	0			
12	2.5	0.5	0.01	2.10	7.5	150	0			
13	2.5	0.75	0.03	1.40	7.5	150	0			
14	2.5	0.75	0.02	1.40	7.5	150	0			
15	2.5	0.75	0.015	1.40	7.5	150	0			
16	2.5	0.75	0.007	1.40	7.5	150	0			
17	2.5	1	0.03	1.05	7.5	150	0			
18	2.5	1	0.025	1.05	7.5	150	0			
19	2.5	1	0.015	1.05	7.5	150	0			
20	2.5	1	0.008	1.05	7.5	150	0			
21	2.5	1.5	0.015	0.70	7.5	150	0			
22	2.5	1.5	0.01	0.70	7.5	150	0			
23	2.5	1.5	0.007	0.70	7.5	150	0			
24	2.5	1.5	0.0035	0.70	7.5	150	0			
25	2.5	2	0.01	0.52	7.5	150	0			
26	2.5	2	0.007	0.52	7.5	150	0			
27	2.5	2	0.005	0.52	7.5	150	0			
28	2.5	2	0.0025	0.52	7.5	150	0			
33	4	0.125	0.125	13.44	7.5	241	0	TN10	TN17	✓
34	4	0.125	0.1	13.44	7.5	241	0			
35	4	0.125	0.065	13.44	7.5	241	0			
36	4	0.125	0.03	13.44	7.5	241	0	TNO4		✓
37	4	0.25	0.125	6.72	7.5	241	0			
38	4	0.25	0.1	6.72	7.5	241	0			
39	4	0.25	0.065	6.72	7.5	241	0			

Test #	U_∞ (m/s)	F_{surge} (Hz)	A_{surge} (m)	Vw	Λ	Ω (rpm)	θ_P	CW	AW	PIV
40	4	0.25	0.035	6.72	7.5	241	0			
41	4	0.5	0.065	3.36	7.5	241	0	TNO3	TN18	✓
42	4	0.5	0.05	3.36	7.5	241	0			
43	4	0.5	0.035	3.36	7.5	241	0			
44	4	0.5	0.015	3.36	7.5	241	0	TNO5		✓
45	4	0.75	0.04	2.24	7.5	241	0			
46	4	0.75	0.03	2.24	7.5	241	0			
47	4	0.75	0.02	2.24	7.5	241	0			
48	4	0.75	0.01	2.24	7.5	241	0			
49	4	1	0.05	1.68	7.5	241	0			
50	4	1	0.035	1.68	7.5	241	0	TNO7	TN19	✓
51	4	1	0.025	1.68	7.5	241	0			
52	4	1	0.01	1.68	7.5	241	0	TN12		✓
53	4	1.5	0.02	1.12	7.5	241	0			
54	4	1.5	0.015	1.12	7.5	241	0			
55	4	1.5	0.01	1.12	7.5	241	0			
56	4	1.5	0.005	1.12	7.5	241	0			
57	4	2	0.015	0.84	7.5	241	0			
58	4	2	0.0125	0.84	7.5	241	0			
59	4	2	0.008	0.84	7.5	241	0	TNO8	TN20	✓
60	4	2	0.004	0.84	7.5	241	0	TNO9		✓
65	6	0.125	0.125	20.16	5.5	265	12.5	TN11		✓
66	6	0.125	0.1	20.16	5.5	265	12.5			
67	6	0.125	0.065	20.16	5.5	265	12.5			
68	6	0.125	0.03	20.16	5.5	265	12.5			
69	6	0.25	0.125	10.08	5.5	265	12.5			
70	6	0.25	0.1	10.08	5.5	265	12.5			
71	6	0.25	0.065	10.08	5.5	265	12.5			
72	6	0.25	0.03	10.08	5.5	265	12.5			
73	6	0.5	0.1	5.04	5.5	265	12.5			
74	6	0.5	0.075	5.04	5.5	265	12.5			
75	6	0.5	0.05	5.04	5.5	265	12.5			
76	6	0.5	0.025	5.04	5.5	265	12.5			
77	6	0.75	0.065	3.36	5.5	265	12.5			
78	6	0.75	0.05	3.36	5.5	265	12.5			
79	6	0.75	0.03	3.36	5.5	265	12.5			

Test #	U_∞ (m/s)	F_{surge} (Hz)	A_{surge} (m)	Vw	Λ	Ω (rpm)	θ_P	CW	AW	PIV
80	6	0.75	0.015	3.36	5.5	265	12.5			
81	6	1	0.07	2.52	5.5	265	12.5			
82	6	1	0.05	2.52	5.5	265	12.5	TN13?		
83	6	1	0.035	2.52	5.5	265	12.5			✓
84	6	1	0.018	2.52	5.5	265	12.5			
85	6	1.5	0.03	1.68	5.5	265	12.5			
86	6	1.5	0.025	1.68	5.5	265	12.5			
87	6	1.5	0.015	1.68	5.5	265	12.5			
88	6	1.5	0.008	1.68	5.5	265	12.5			
90	6	2	0.015	1.26	5.5	265	12.5	?		
91	6	2	0.0125	1.26	5.5	265	12.5	TN14		✓
92	6	2	0.006	1.26	5.5	265	12.5	?		

For the simulations, the rotational speed used was 240 rpm instead of 241 rpm to ensure the periodic behavior of the rotor azimuth angle for a given platform position.

A.5 Surge-Oscillation Tests Performed by Polimi in the Follow-On Campaign

Table A-5. Surge Motion Tests (No Control)

Load Case	U'_∞ (m/s)	F_{surge} (Hz)	A_{surge} (deg)	Ω (rpm)	θ_P (deg)
2.1	4.19	0.125	0.125	240	0
2.5	4.19	1.0	0.035	240	0
2.7	4.19	2.0	0.008	240	0
2.9	6.03	0.125	0.125	265	12.5
2.10	6.03	1.0	0.035	265	12.5
2.11	6.03	2.0	0.0125	265	12.5

A.6 Pitch-Oscillation Tests Performed by Polimi in the Follow-On Campaign

Table A-6. Pitch Motion Tests (No Control)

Load Case	U'_∞ (m/s)	F_{surge} (Hz)	A_{surge} (deg)	Ω (rpm)	θ_P (deg)
3.1	4.19	0.125	3.000	240	0
3.2	4.19	0.125	1.200	240	0
3.3	4.19	0.5	0.600	240	0

Load Case	U'_∞ (m/s)	F_{surge} (Hz)	A_{surge} (deg)	Ω (rpm)	θ_P (deg)
3.5	4.19	1.0	1.400	240	0
3.6	4.19	1.0	0.400	240	0
3.7	4.19	2.0	0.300	240	0
3.8	4.19	2.0	0.160	240	0
3.9	6.03	0.125	3.000	265	12.5
3.10	6.03	1.0	1.500	265	12.5
3.11	6.03	2.0	0.500	265	12.5

A.7 Tower Influence

One small sensitivity analysis was performed in OpenFAST. Figure A-1 shows the aerodynamic thrust force (*Fx*) at the hub location when accounting and not accounting for the tower shadow effect.

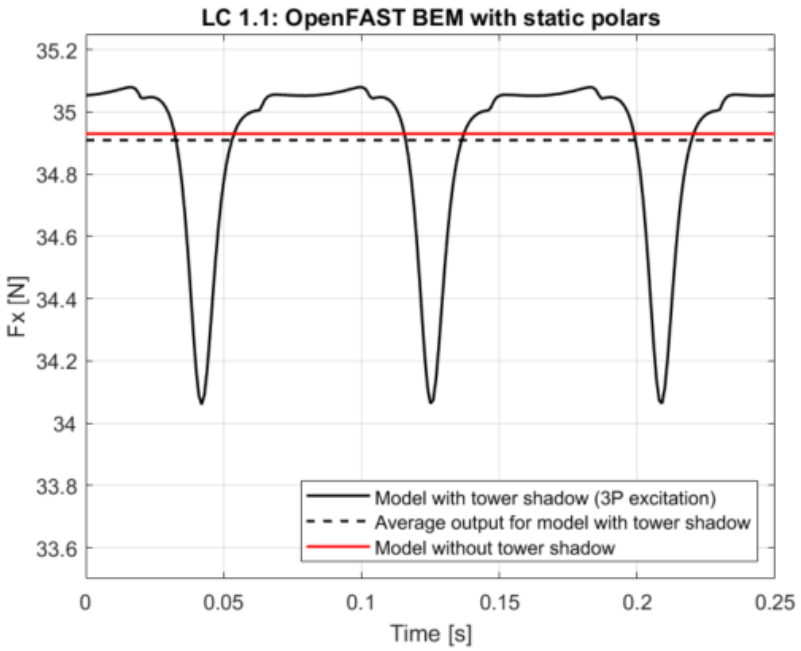

Figure A-1. Tower influence over the aerodynamic thrust force (*Fx*) at hub location for one rotor revolution

When the tower shadow is included in the numerical model, the system experiences a 3P excitation (black line in Figure A-1). This excitation corresponds to the three blades passing in front of the tower for one revolution. The resulting average value (denoted with a dashed black line) can be considered equivalent to the output when the tower shadow is not included (red line).